Sea Level Rise and Urban Infrastructure

By ALLAN HSIAO*

How exposed are cities to the threat of sea level rise? I quantify this exposure worldwide with a focus on urban infrastructure. I document three facts. First, Asian cities are highly exposed. Second, poorer cities and neighborhoods are less exposed. Third, exposure accelerates as sea level rise passes 1.5 meters.

I. Data

I compile global data on sea level rise (SLR) and urban infrastructure at a granular resolution of 30 meters (m). The data cover 11,422 cities with a total population of 3.7 billion.

A. Sea level rise

The Intergovernmental Panel on Climate Change (IPCC) projects 0.38 to 0.77 m of global mean SLR by 2100 (Fox-Kemper et al., 2021). Projections exceed 2 m in worst-case scenarios with faster-than-projected ice loss in Antarctica and Greenland. And for many coastal cities, land subsidence leads to a sinking coastline that adds to SLR in relative terms. The worst-affected cities – largely concentrated in Asia – are sinking between 5 and 15 millimeters (mm) per year (Tay et al., 2022).

I use elevation data and a simple physical model to assess inundation risk under SLR of up to 5 m. Global elevation data at 30-m resolution come from the DeltaDTM Global Coastal Digital Terrain Model, which isolates the bare-earth surface of coastal areas (Pronk et al., 2024). These data cover the Low Elevation Coastal Zone (LECZ), defined as low-lying coastal areas with elevation less than 10 m above mean sea level, and they aim to remove elevation bias from the Copernicus GLO-30 Digital Surface Model, which does not separate forests and buildings from bare-earth surface. The Copernicus data derive from satellite measurements taken on the TanDEM-X mission from 2011 to 2015, and they include a water body mask that distinguishes land from ocean, lakes, and rivers.

For a cell i, I thus observe elevation e_i and ocean indicator o_i. I model inundation $n_i(s)$ under SLR scenario s by applying the principle of hydrological connectivity (Bracken et al., 2013). I simulate the ocean's path as follows. First, I mark current ocean cells as inundated.

$$n_i(s) = o_i$$

Second, I mark cells as inundated if they are (a) adjacent to an inundated cell and (b) below sea level.

$$n_i'(s) = a_i(s) \cdot b_i(s),$$
$$a_i(s) = \mathbb{1}\left[\sum_j a_{ij} n_j(s) > 0\right],$$
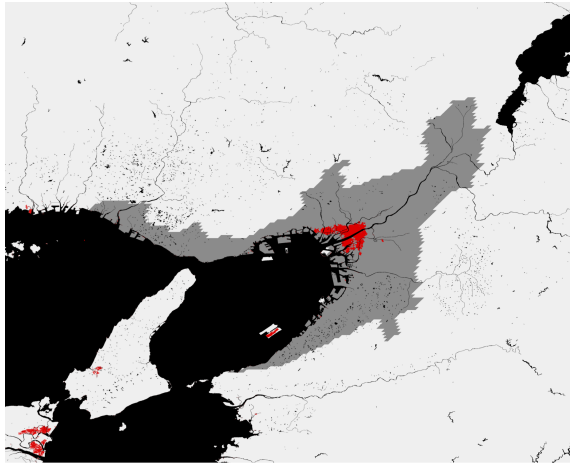$$b_i(s) = \mathbb{1}[e_i < s],$$

where a_{ij} records whether cells i and j are adjacent, including diagonally. Third, I repeat until I identify all inundated cells. I do so in increments of 0.1 m for SLR scenarios between 0 and 5 m, assuming no inundation for cells outside of the LECZ or more than 500 kilometers (km) inland.

The model captures permanent risk under SLR. SLR is a relative quantity: inundation depends on land elevation above sea level, and so it occurs whether the sea rises or the land sinks. Cities thus experience SLR as the sum of global mean SLR and local land subsidence. Fast-subsiding cities experience each SLR scenario before slow-subsiding cities do.

The model does not capture temporary risk from tides and storm surges. Evaluating such risk requires more sophisticated modeling because it must account for drainage, which depends on runoff responses, soil characteristics, land use, and other hydrological factors. Permanent risk is simpler because drainage is not possible for land that lies permanently in the ocean's path. Flood defenses can alter the ocean's path, but the model does not capture such forms of current or future adaptation. Indeed, while many

* Stanford University, Department of Economics, 579 Jane Stanford Way, Stanford, CA 94305, ajhsiao@stanford.edu. Xilin Fan provided exceptional research assistance.

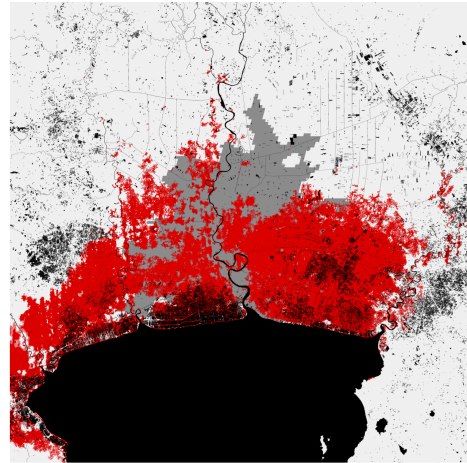*A. Osaka under SLR of 1 m*   *B. Bangkok under SLR of 2 m*

FIGURE 1. INUNDATION

Note: Each map has four colors. Black is ocean, rivers, and lakes, dark gray is land within the urban boundary, and light gray is other land. Red is model-predicted inundation risk under SLR of 1 m on the left and 2 m on the right.

Dutch cities lie below sea level, the Netherlands has adapted with flood defense at national scale. I interpret the model as identifying inundation risk rather than inundation itself.

Figure 1 illustrates for two of the most exposed cities in the world. On the left, under SLR of 1 m, inundation risk for Osaka is concentrated at the mouth of the Yodo river delta. Areas farther upstream remain unexposed, as does much of the rest of Osaka Bay. On the right, under SLR of 2 m, much of Bangkok is at risk of inundation. The risk is not restricted to the riverbanks of the Chao Phraya, extending instead throughout the Bay of Bangkok.

B. Urban infrastructure

Urban boundaries at 1-km resolution come from the Global Human Settlement Layer Urban Center Database (GHS-UCDB) (Uhl et al., 2024). These boundaries delineate urban clusters, which I refer to as "cities," of contiguous cells with population densities of at least 1,500 per km^2 and total populations of at least 50,000 in 2025. Granular population data are derived from build-up surface data, as extracted from Landsat and Sentinel-2 satellite imagery. The most populous cities are the Guangzhou, Jakarta, and Dhaka metropolitan areas with populations of 43.0, 40.5, and 37.3 million. The largest cities are Dhaka, Guangzhou, and Tokyo with land areas of 6,611, 6,454, and 5,165 km^2.

The average city has a population of 322,654 and an area of 57 km^2. I refine these boundaries with the water body mask of 30-m resolution by dropping ocean, lake, and river cells.

For each city, I compile geocoded data on education, health, and transport infrastructure. Education and health data come from OpenStreetMap. The data record schools, kindergartens, colleges, universities, hospitals, clinics, doctor practices, dentist practices, and pharmacies in 2024, where schools include primary, middle, and high schools but do not distinguish among them. Transport data come from the Global Roads Inventory Project (GRIP). The data record highways, primary, secondary, and tertiary roads with the most recent temporal coverage available when assembled in 2018.

I study heterogeneity by income both across and within cities. Across cities, I measure 2020 GDP by country with GHS-UCDB data. Higher-income cities are those in countries with above-median GDP relative to other countries. Within cities, I proxy with 2023 night light intensity by cell with Earth Observation Group (EOG) data, which derive from Visible Infrared Imaging Radiometer Suite (VIIRS) satellite measures. Higher-income neighborhoods are cells with above-median night light intensity relative to other cells in the same city. I downscale the data from 450-m to 30-m resolution.

TABLE 1—INFRASTRUCTURE EXPOSURE

Rank	SLR of 1 m		SLR of 2 m		SLR of 3 m	
	City	%	City	%	City	%
1	Osaka	4.8	Bangkok	55.5	Bangkok	94.4
2	Jakarta	2.2	Shanghai	19.0	Shanghai	80.2
3	Tokyo	2.2	Manila	11.8	Suzhou	31.3
4	Lagos	1.7	Osaka	9.9	Lagos	25.7
5	Mumbai	1.1	Jakarta	9.5	Manila	21.3
6	Manila	1.0	Lagos	9.0	Ho Chi Minh City	20.9
7	New York City	0.4	Tokyo	5.4	Kolkata	20.1
8	Suzhou	0.2	Ho Chi Minh City	4.0	Jakarta	16.3
9	Bangkok	0.2	Kolkata	3.8	Osaka	15.7
10	Shanghai	0.2	New York City	2.7	Guangzhou	12.5

Note: I list the ten most exposed cities under SLR of 1, 2, and 3 m. For each SLR scenario, I compute the percentage of education, health, and transport infrastructure that is exposed to inundation. Education infrastructure is schools, health is hospitals and clinics, and transport is highways and primary roads. I compute education, health, and transport percentages separately, then I take the average to obtain a single infrastructure percentage.

II. Exposure

I compute the percentage of urban land and infrastructure at risk of inundation under a range of SLR scenarios.

A. Asian cities are highly exposed

For a given SLR scenario, I compute the percentage of education, health, and transport infrastructure at risk of inundation in each city. Education infrastructure is schools, health is hospitals and clinics, and transport is highways and primary roads. Primary, middle, and high schools are pooled in the data, and each facility has implicitly equal weight. I similarly pool hospitals and clinics, as well as highways and primary roads. I define infrastructure exposure as the average of these education, health, and transport percentages.

Table 1 presents the ten most exposed cities under SLR of 1, 2, and 3 m. Asian cities dominate each list. Under SLR of 1 m, 4.8% of Osaka's infrastructure is at risk of inundation. Jakarta and Tokyo follow with 2.2% exposure, and Lagos and New York City enter as the only non-Asian cities. Under SLR of 2 m, Bangkok, Shanghai, and Manila rise to the top. Most of Bangkok's infrastructure is at risk, and Lagos and New York City remain the only non-Asian cities. Under SLR of 3 m, Bangkok, Shanghai, and Suzhou are most exposed. Inundation threatens nearly all infrastructure in Bangkok and the vast majority in Shanghai. Chinese cities occupy two of the top three and three of the top ten positions. Lagos is the only non-Asian city.

B. Poorer cities and neighborhoods are less exposed

I assess exposure for lower-income cities and neighborhoods. I identify lower-income cities based on country-level GDP, and I aggregate as follows. For land, I sum the at-risk and total areas weighting by population density, and I take the ratio to obtain aggregate land exposure.

$$\bar{e} = \frac{\sum_c p_c x_c}{\sum_c p_c X_c},$$

where cities c have population density p_c, at-risk land area x_c, and total land area X_c. For infrastructure, I compute the same measure separately for education, health, and transport, then I average the three to obtain aggregate infrastructure exposure. Similarly, I identify lower-income neighborhoods based on cell-level night light intensity, and I aggregate analogously. I repeat with higher-income cities and neighborhoods for comparison.

Figure 2A shows that land and infrastructure are less exposed in lower-income cities, relative to higher-income cities, at all levels of SLR. The reason is that higher-income cities are more
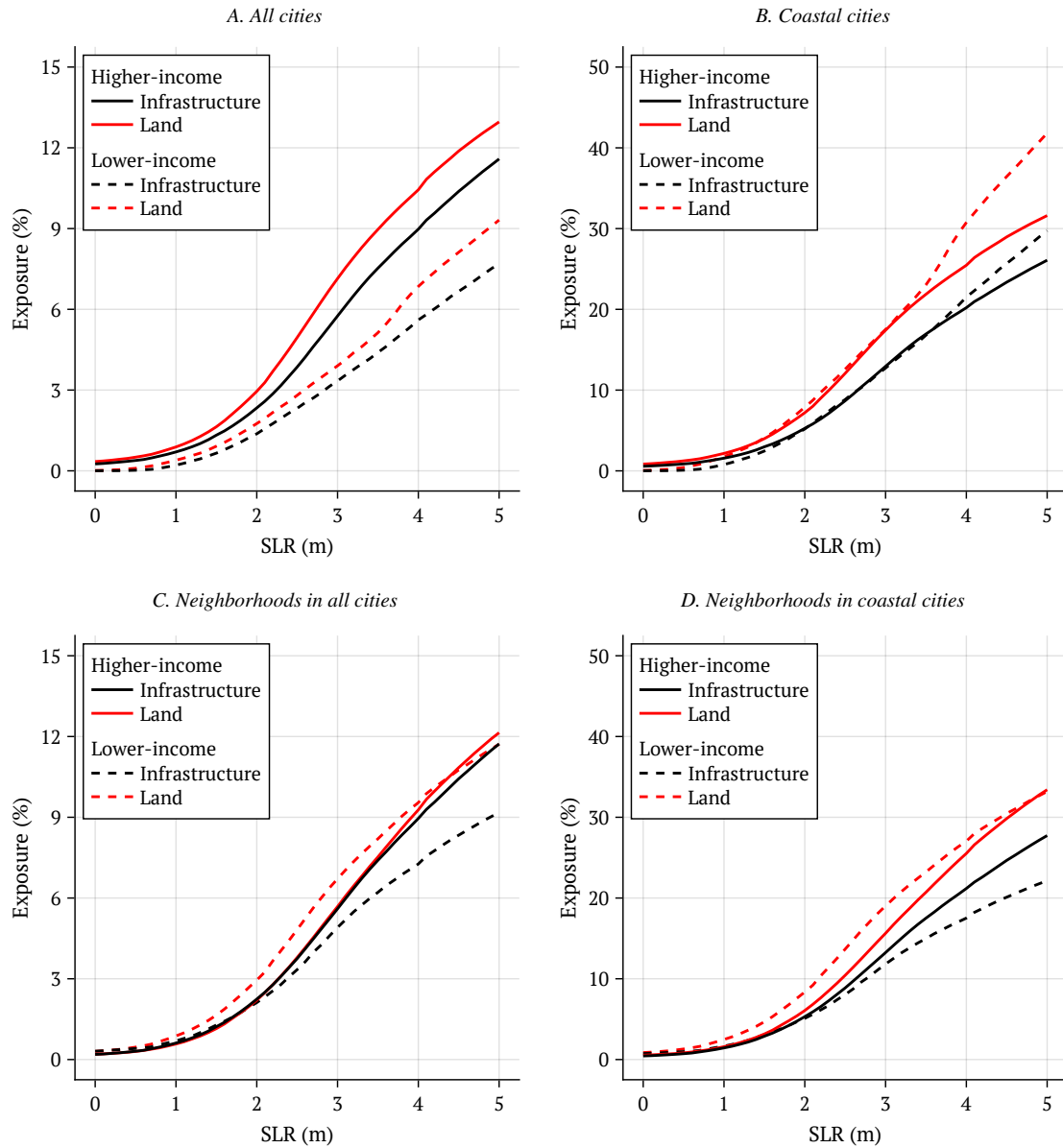
A. All cities

B. Coastal cities

C. Neighborhoods in all cities

D. Neighborhoods in coastal cities

FIGURE 2. HETEROGENEITY BY INCOME

Note: The *y*-axes show the percentage of land or infrasture exposed to inundation under SLR. The *x*-axes show SLR scenarios of increasing severity. Land is land area within each urban boundary. Infrastructure includes education, health, and transport. Education infrastructure is schools, health is hospitals and clinics, and transport is highways and primary roads. Lower-income cities are cities in countries with below-median GDP relative to other countries, while higher-income cities are above-median. Lower-income neighborhoods are cells with below-median night light intensity relative to other cells in the same city, while higher-income neighborhoods are above-median. Figures A and C include all 11,422 cities. Figures B and D are restricted to the 2,087 coastal cities that face some degree of land inundation under SLR of 5 m. The *y*-axis has a smaller scale in figures A and C and a larger scale in figures B and D.

likely to be coastal. Figure 2B conditions on coastal cities, which I define as cities with any land at risk of inundation under SLR of 5 m. I identify 2,087 such cities. Lower- and higher-income cities are similarly exposed until SLR passes 3.5 m, when lower-income exposure ac-

celerates and surpasses higher-income exposure.

Figure 2C shows that lower-income neighborhoods have less infrastructure exposure than higher-income neighborhoods, despite having more land exposure. The reason is that infrastructure is relatively well-placed in lower-

income neighborhoods. In higher-income neighborhoods, infrastructure exposure aligns with land exposure because infrastructure is spread evenly over space. In lower-income neighborhoods, infrastructure exposure does not rise as quickly as land exposure because infrastructure is concentrated on relatively safe land. Figure 2D shows that this pattern persists for coastal cities, where the gap between land and infrastructure exposure is even larger for lower-income neighborhoods. The pattern also emerges for higher-income neighborhoods, but to a lesser extent.

C. *Exposure accelerates as SLR passes 1.5 m*

Each curve in figure 2 features an inflection point around SLR of 1.5 m. As SLR increases from 0 to 1.5 m, inundation risk rises at a modest pace. And it remains at modest levels: under SLR of 1.5 m, average infrastructure exposure is 1.2% for the sample of all cities and 2.9% for the sample of coastal cities. As SLR increases beyond 1.5 m, inundation risk rises at a more rapid pace. And it reaches relatively high levels: under SLR of 5 m, average infrastructure is 11.1% for all cities and 26.4% for coastal cities.

III. Implications

Cities should aim to slow local land subsidence. Global mean SLR is beyond the control of any particular city, but it is likely to remain between 0 and 1.5 m by 2100. I show that exposure is more limited in this range. SLR beyond this range will be driven by local land subsidence, which cities can influence with policy. Of course, doing so is not trivial. A leading cause of land subsidence is groundwater extraction, often in cities with few alternative water sources. Asian cities are subsiding at particularly high rates (Tay et al., 2022). I show that these same cities are especially vulnerable to the inundation that potentially follows.

These cities also offer insights. Rapid land subsidence has placed Jakarta at the forefront of navigating the threat of SLR. It provides an important setting for studying the challenges of urban adaptation (Hsiao, 2023) and the consequences for urban inequality (Hsiao, 2024). More broadly, how can cities adapt? And how can governments help? These are the key questions facing the people and politicians of our coastal cities.

REFERENCES

Bracken, Louise, John Wainwright, Geneviève Ali, Dörthe Tetzlaff, Mark Smith, Sim Reaney, and André Roy. 2013. "Concepts of Hydrological Connectivity: Research Approaches, Pathways and Future Agendas." *Earth-Science Reviews*, 119: 17–34.

Fox-Kemper, Baylor, Helene Hewitt, Cunde Xiao, et al. 2021. "Ocean, Cryosphere and Sea Level Change." In *Climate Change 2021: The Physical Science Basis. Contribution of Working Group I to the Sixth Assessment Report of the Intergovernmental Panel on Climate Change*. Chapter 9, 1211–1362. Cambridge University Press.

Hsiao, Allan. 2023. "Sea Level Rise and Urban Adaptation in Jakarta."

Hsiao, Allan. 2024. "Sea Level Rise and Urban Inequality." *AEA Papers and Proceedings*, 114: 47–51.

Pronk, Maarten, Aljosja Hooijer, Dirk Eilander, Arjen Haag, Tjalling de Jong, Michalis Vousdoukas, Ronald Vernimmen, Hugo Ledoux, and Marieke Eleveld. 2024. "DeltaDTM: A Global Coastal Digital Terrain Model." *Scientific Data*, 11: 273.

Tay, Cheryl, Eric Lindsey, Shi Tong Chin, Jamie McCaughey, David Bekaert, Michele Nguyen, Hook Hua, Gerald Manipon, Mohammed Karim, Benjamin Horton, Tanghua Li, and Emma Hill. 2022. "Sea-Level Rise from Land Subsidence in Major Coastal Cities." *Nature Sustainability*, 5(12): 1049–1057.

Uhl, Johannes, Martino Pesaresi, Luca Maffenini, Patrizia Sulis, Monica Crippa, Diego Guizzardi, Enrico Pisoni, Claudio Belis, Duarte Oom, Alfredo Branco, Dennis Mwaniki, Edwin Kochulem, Daniel Githira, Alessandra Carioli, Daniele Ehrlich, Pierpaolo Tommasi, Thomas Kemper, and Lewis Dijkstra. 2024. "Stats in the City GHSL Urban Centre Database 2025."